

Study of the Cost Reductions Achievable from the Novel SARC CO₂ Capture Concept Using a Validated Reactor Model

Chaitanya Dhoke, Schalk Cloete, Shahriar Amini, and Abdelghafour Zaabout*

Cite This: *Ind. Eng. Chem. Res.* 2021, 60, 12390–12402

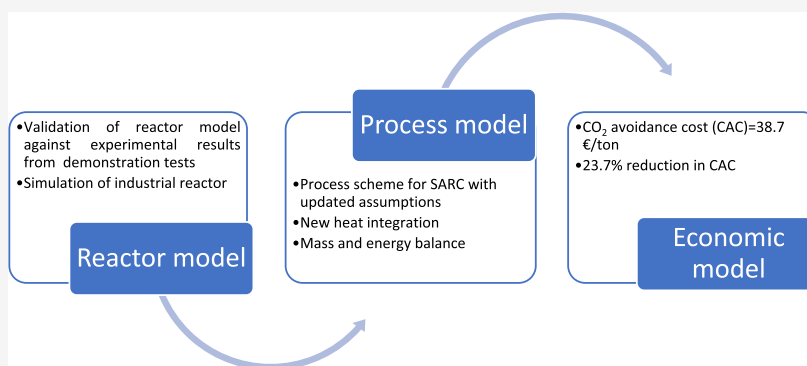
Read Online

ACCESS |

Metrics & More

Article Recommendations

Supporting Information



ABSTRACT: New process concepts, such as the swing adsorption reactor cluster (SARC) CO₂ capture process, are often technoeconomically investigated using idealized modeling assumptions. This study quantifies the impact of this practice by updating a previous economic assessment with results from an improved reactor model validated against recently completed SARC lab-scale demonstration experiments. The experimental comparison showed that the assumption of chemical equilibrium was valid, that the previously employed heat transfer coefficient was conservatively low, and that the required reduction of axial mixing could be easily achieved using simple perforated plates in the reactor. However, the assumption of insignificant effects of the hydrostatic pressure gradient needed to be revised. In the economic assessment, the negative effect of the hydrostatic pressure gradient was almost canceled out by deploying the experimentally observed heat transfer coefficients, resulting in a small net increase in CO₂ avoidance costs of 2.8–4.8% relative to the unvalidated model. Further reductions in axial mixing via more perforated plates only brought minor benefits, but a shorter reactor enabled by the fast experimentally observed adsorption kinetics had a larger positive effect: halving the reactor height reduced CO₂ avoidance costs by 13.3%. A new heat integration scheme feeding vacuum pressure steam raised from several low-grade heat sources to the SARC desorption step resulted in similar gains. When all improvements were combined, the optimal CO₂ avoidance cost was 23.7% below the best result from prior works. The main uncertainty that needs to be overcome to realize the great economic potential of the SARC concept is long-term sorbent stability: mechanical stability must be improved substantially and long-term chemical stability under real flue gas conditions must be demonstrated.

1. INTRODUCTION

Low-temperature adsorption-based CO₂ capture is attracting growing attention as a promising technology with great prospects for reducing CO₂ capture costs from stationary industrial sources.^{1,2} One of the main advantages of this technology is its retrofitting flexibility to different industrial CO₂ sources as it provides: (i) several regeneration options that can use electrical or thermal energy sources depending on availability in the targeted industry, (ii) the possibility of heat integration with the host site when cheap heat waste is available, and (iii) a wide variety of sorbents suitable to the wide range of CO₂ partial pressure in the flue gas of the different targeted industries. The largest research focus in this field remains on sorbent development, from the aspects of reducing the heat of reaction, increasing the adsorption capacity, and improving the sorbent tolerance and stability

under industrial flue gases containing impurities such as SO_x and NO_x.^{1–3} Thousands of sorbents have been proposed under several different families bringing different strengths and weaknesses to adsorption-based CO₂ capture technology. A comprehensive review on sorbent development can be found in references 1, 4, 5.

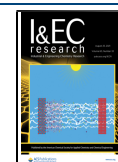
The wide variety of proposed sorbents could complicate the mission of identifying the best ones for the different industrial

Received: January 26, 2021

Revised: July 29, 2021

Accepted: July 30, 2021

Published: August 10, 2021



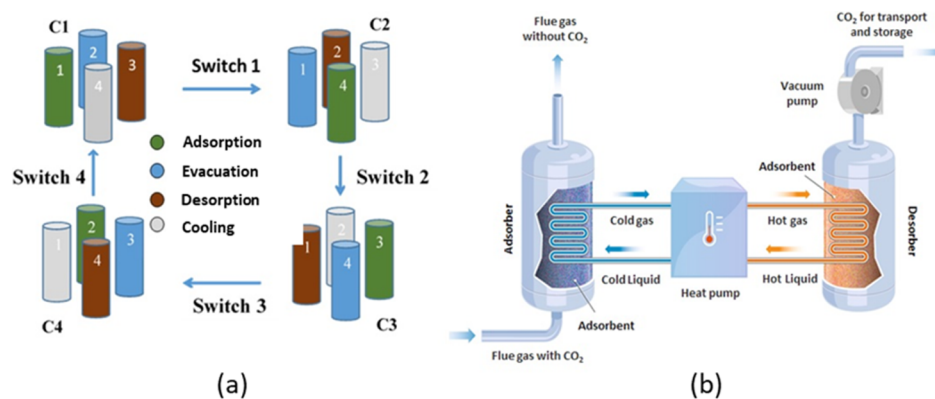


Figure 1. Conceptual design of SARC: (a) a SARC cluster composed of four reactors for steady operation; (b) a heat pump transferring heat between two SARC reactors in the cluster; one under adsorption and the other under desorption. Reprinted from Dhoke et al.,²⁵ page 2, Copyright 2020, with permission from Elsevier.

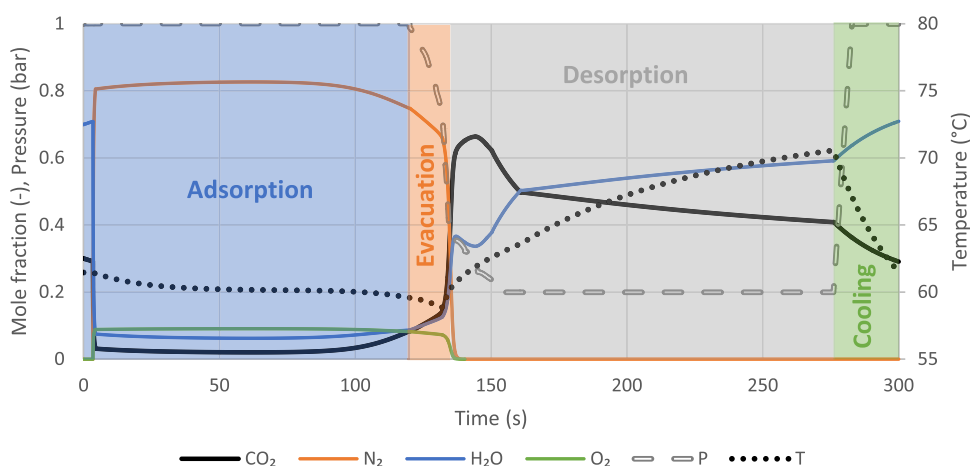


Figure 2. SARC cycle for the optimal large-scale case simulated in this study.

flue gasses, but attempts were made in proposing preliminary screening methodologies that link the sorbent to the overall process performance and costs.⁶ More importantly, it is increasingly acknowledged that a suitable contacting system is key for extracting the full potential of the technology, suggesting that the sorbent and reactor development should be tightly linked to bring the targeted significant cost reduction.^{1,3}

Several reactor systems have been proposed for adsorption-based CO₂ capture, each associated with strengths and weaknesses.⁷ Fixed bed was the most studied configuration,^{8,9} owing to its simplicity, but the associated high pressure drop and high mass and heat transfer resistance reduce its attractiveness for widespread industrial scale deployment. Other configurations such as monolithic,¹⁰ structured,¹¹ rotating,¹² and moving^{13–15} beds are attracting increased research attention given their ability to minimize the reported challenges of fixed bed. On the other extreme, the fluidized bed-based configuration alleviates the high mass and heat transfer resistance and the high pressure drop drawbacks of fixed beds. However, the associated good mixing is not suitable for the equilibrium-based adsorption reactions involved in the process, resulting in early breakthrough of CO₂ that substantially reduces the CO₂ recovery rate of the process.^{16,17} The multistage counter-current circulating configuration has shown promise to minimize the negative effect of the good mixing feature of fluidized bed,^{18–21} making it a very attractive configuration for further scale-up and commercial implemen-

tation. As discussed in the next section, the technology investigated in this study seeks to combine the simplicity of fixed beds with the good mixing of fluidized beds, using the multistage configuration to achieve good CO₂ capture performance.

1.1. Swing Adsorption Reactor Cluster (SARC). SARC is an adsorption-based CO₂ capture that employs a cluster of multistage fluidized bed reactors, each one cycling different steps to complete capture CO₂ from stationary source and deliver concentrated CO₂ ready for storage or utilization (Figure 1a). The reactors are operated in the bubbling/turbulent fluidized bed condition facilitating implementing a hybrid regeneration mode combining temperature and vacuum swings in addition to efficient heat integration using heat pump to minimize the energy penalty. This concept removes the energy released during adsorption using the heat pump and supplies it to the desorption step (Figure 1b), thus bringing substantial energy savings²² and cost reductions²³ of CO₂ capture. A simple perforated plate arrangement was used to create separated chambers (referred to as multistage fluidized bed) in each reactor to reduce the extent of back mixing.²⁴ This provides the multistage effect required to delay the breakthrough of CO₂ during adsorption. The SARC technology is particularly suited for retrofitting in industrial stationary CO₂ sources where large quantities of steam are not available as it requires only electrical energy input and does not depend on heat integration with the host process.

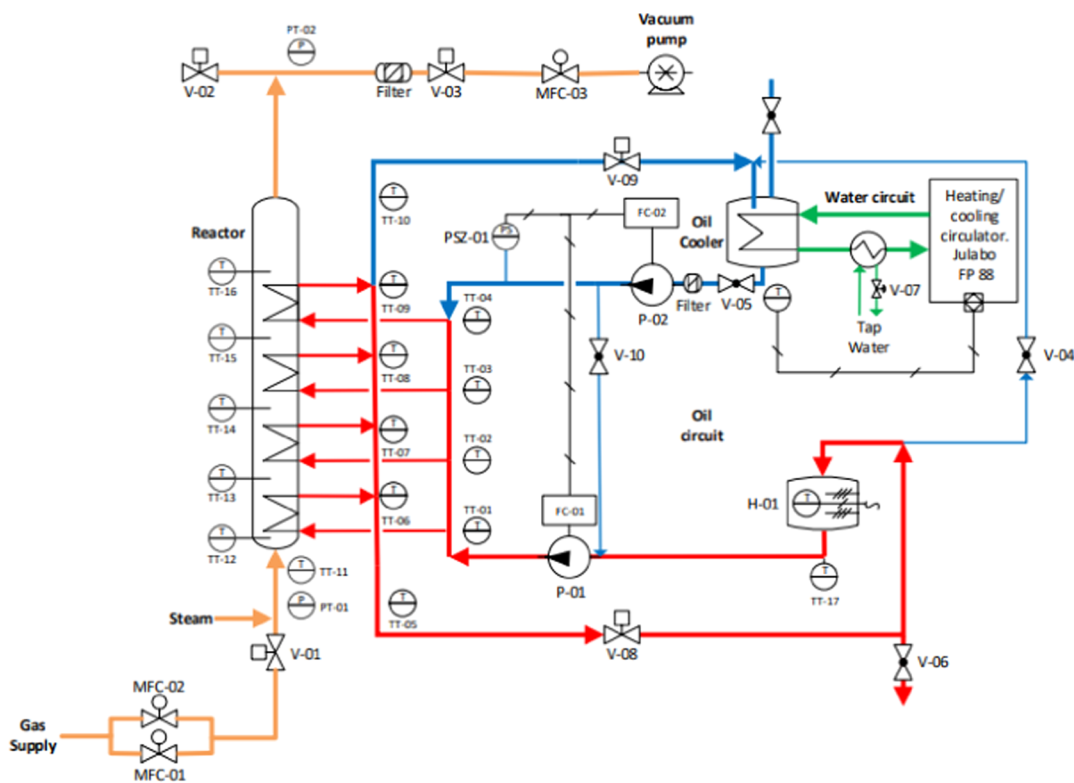


Figure 3. Process flow scheme of the SARC experimental setup. Reprinted from ref 24 Copyright 2020, with permission from American Chemical Society.

An illustration of the SARC cycle in a simulated four-stage SARC reactor using a PEI-based sorbent is presented in Figure 2 showing the four steps involved (adsorption, evacuation, desorption, and cooling). In the adsorption step, the sorbent adsorbs CO_2 from the flue gas at atmospheric pressure (1 bar) and low temperatures ($\sim 60^\circ\text{C}$). The N_2 accumulated in the reactor during the adsorption step is evacuated and vented to the atmosphere in the evacuation step to improve the purity of CO_2 . This is done by reducing the pressure to a moderate level (~ 400 mbar). In the desorption step, a temperature swing using the heat pump is applied combined with a stronger vacuum to recover the CO_2 adsorbed in the first step. Finally, a cooling and repressurization of the reactor is applied to reduce the temperature to the level required to start the next SARC cycle. The SARC proof of concept was demonstrated²⁵ and suitable sorbents were identified.²⁶

1.2. Novelty of the Study. Previous techno-economic assessment studies on the SARC technology have revealed competitive performance in terms of energy efficiency and cost against benchmarking technologies for capturing CO_2 from both coal^{20,27} and cement.^{22,23} However, the SARC reactor behavior was modeled using several assumptions that have not yet been validated, introducing significant uncertainty. Thus, it is necessary to validate these assumptions to determine with greater confidence whether the SARC concept is suitable for scale-up. This study presents the required model validation against recently completed SARC lab-scale demonstration experiments. Based on this validation exercise, the model is improved and used to update the economic performance estimates of the SARC concept applied to CO_2 capture from cement production. An additional novelty in this work is the introduction of a new heat integration scheme to utilize various sources of low-grade heat in the SARC plant for raising

vacuum pressure steam to aid in sorbent regeneration. Productive utilization of this low-grade heat that was rejected in previous studies improves the SARC energy efficiency and economic performance. Next to this new process configuration, another promising opportunity and a key challenge are identified and quantified. The opportunity revolves around the experimental finding that equilibrium conversion could be attained with significantly shorter gas residence times than assumed in previous simulation studies allowing for a significant shortening of the reactor. Sorbent durability is the main challenge identified in this work, and dedicated sorbent development work is recommended to reduce the attrition rate.

2. METHODOLOGY

2.1. Experimental Setup. A lab-scale experimental setup was built to demonstrate the SARC concept as detailed in a previous study.²⁴ The process flow scheme of the rig is presented in Figure 3. The setup comprises a multistage fluidized bed reactor with in-built heat exchanger, the oil and water circuits controlling the heat exchange, a vacuum pump, three mass flow controllers, and various thermocouples and pressure sensors. The details of the experimental setup and operation are presented in the Supporting Information included with this paper.

2.2. Experimental Procedure. The experimental campaign composed of breakthrough experiments and full SARC cycles using a polyethyleneimine-based (EB-PEI) sorbent to capture around 90% of CO_2 . Adsorption in the breakthrough experiment was carried out with a fully regenerated sorbent while in the SARC cycle it started with a partially regenerated sorbent. In both the experiments, adsorption was completed at

60 °C with 12.5% of CO₂ in N₂ and atmospheric pressure. The experimental conditions are presented in Table 1.

Table 1. Experimental Conditions

parameters	values
superficial velocity (m/s) during adsorption	0.19
particle density (g/mL)	1.36
particle size (μm)	145
sorbent loading (kg)	11.8
fluidization regime	bubbling

The overall heat transfer coefficient from each stage (h_i) was measured for all four steps of the SARC concept using eq 1. The heat transfer coefficient mentioned in this study refers to the overall heat transfer coefficient.

$$h_i = \frac{\dot{m}_{\text{oil}} \times c_{p,\text{oil}} \times (T_{\text{oil}}^{\text{out}} - T_{\text{oil}}^{\text{in}})}{A \times \left(T_{\text{bed}} - \left(\frac{T_{\text{oil}}^{\text{out}} + T_{\text{oil}}^{\text{in}}}{2} \right) \right)} \quad (1)$$

Here, \dot{m}_{oil} is the mass flow rate of oil (kg/s), $c_{p,\text{oil}}$ is the oil specific heat capacity

(J/(kg K)), $T_{\text{oil}}^{\text{in}}$ and $T_{\text{oil}}^{\text{out}}$ are the oil inlet and outlet temperatures (°C), respectively, T_{bed} is the bed temperature (°C), and A is the heat transfer area (m²).

The average overall heat transfer coefficient (H_i) in the different reactor steps (e.g., adsorption or desorption) was then estimated from the instantaneous heat transfer coefficient and the heat transfer rate in each stage.

$$H_i = \frac{\sum (h_i \times q_i)}{\sum q_i} \quad (2)$$

Here, h_i is the instantaneous overall heat transfer coefficient calculated from eq 1 for i^{th} stage (W/(m² K)) and q_i is the heat transfer rate for the i^{th} stage (W).

More details about the experimental procedure and campaign can be found in the previous publication.²⁴ The results from these two studies were used to validate the reactor model as described below.

2.3. Reactor Modeling. The multistage SARC reactor is simulated as a series of continuous stirred tank reactors (CSTRs) using an in-house Matlab code first introduced by Zaabout et al.²⁰ and subsequently deployed in several follow-up studies.^{22,23,27} Transient mass and energy balances are solved for each CSTR in series, assuming that thermal and chemical equilibrium is reached in each CSTR. Gas travels from one CSTR to the next, whereas the solids phase remains fixed in each CSTR. Regarding chemical equilibrium, CO₂ and H₂O isotherms for the PEI sorbent were derived in a previous work.²⁶ A typical SARC cycle simulated by this model is depicted in Figure 2.

In the present study, this CSTR-in-series model will be used for two purposes: (1) validation against the experimental results from the lab-scale SARC unit and (2) large-scale simulations to quantify the change in the energy penalty and CO₂ avoidance cost when implementing the learnings from the validation exercise in the large-scale SARC simulations.

The most important modification to the model made for the present work was the inclusion of the previously neglected hydrostatic pressure gradient in the bed. This will increase the pressure in the lower reactor stages, increasing CO₂ adsorption

and inhibiting CO₂ desorption. Due to the shape of the CO₂ adsorption isotherm, the negative effect during desorption will outweigh the positive effect during adsorption, increasing the energy penalty of the SARC concept.

Furthermore, the description of heat transfer differs significantly between the reactor simulations for validation and for large-scale process modeling. In the large-scale cases, heat transfer is modeled as in our previous studies, assuming a heat pump with a working fluid condensing and evaporating at specified constant temperatures when heating and cooling the reactor. Here, eq 3 shows that the heat transfer is driven by a constant heat transfer coefficient (h), a heat transfer surface area (A), and a varying temperature difference between the condensing or evaporating heat pump working fluid (T_{wf}) and the bed in each stage of the reactor (T_{bed}).

In the validation cases, however, the heat transfer was carried out using heating oil without phase change. Hence, the oil outlet temperature changed relative to the inlet temperature, depending on the rate of heat transfer, changing the average working fluid temperature. In this case, eq 3 was modified on the assumption that the working fluid temperature is the average between the inlet and outlet temperatures. Eq 4 shows the resulting equation, accounting for the finite flow rate of the heating oil (\dot{m}_{oil}). It is clear that, if the heating oil flow rate approaches infinity, the denominator approaches unity and eq 4 becomes identical to eq 3 because the heating oil outlet temperature would be equal to the inlet temperature ($T_{\text{oil}}^{\text{in}}$). However, for a finite heating oil flow rate, the heat transfer rate will reduce because the average heating oil temperature will be closer to the reactor temperature. If the heating oil flow rate approaches zero, so does the heat transfer rate.

$$q_{\text{large}} = hA(T_{\text{wf}} - T_{\text{bed}}) \quad (3)$$

$$q_{\text{lab}} = \frac{hA(T_{\text{oil}}^{\text{in}} - T_{\text{bed}})}{1 + \frac{hA}{2\dot{m}_{\text{oil}}c_{p,\text{oil}}}} \quad (4)$$

The heat transfer coefficient was assumed constant for all reactor stages in all SARC steps for the large-scale simulations. However, dedicated heat transfer coefficients were derived for different stages and steps to maximize accuracy in the lab-scale simulations. These heat transfer coefficients are specified in the Results and Discussion section.

2.4. Process Modeling. For the large-scale process modeling, the reactor model was run to achieve 90% CO₂ capture and 96% CO₂ purity using 2000 m² of heat transfer surface area per reactor and 0.1 bar desorption pressure. These conditions are identical to case 1 in Cloete et al.,²³ which proved to be the most economical case investigated for CO₂ capture from a cement plant.

The reactor model provided the flow rates and compositions of the streams exiting each step in the SARC cycle, the total heat transfer rate through the heat pump, the heat pump evaporation and condensation temperatures, and the evacuation pump pressure. This information was then used in the process model modeled in Aspen plus to calculate the power consumption of the heat pump and the two vacuum pumps (large pump for desorption and small pump for evacuation). In addition, the power consumption for CO₂ compression, the blower to overcome the pressure drop in the reactor (weight of the fluidized particles plus 10% for the gas distributor) and auxiliaries (mainly water pumps) is also calculated from the

process simulation. The assumptions made in the process modeling are presented in Table 2.

Table 2. Assumption Used in Process Model^a

SARC process	
heat pump compressor isentropic efficiency, %	85
heat pump compressor electric-mechanical efficiency, %	94
vacuum pump isentropic efficiency, %	85
vacuum pump electrical-mechanical efficiency, %	95
vacuum pump intercooling temperature, °C	35
regenerator recycle fan isentropic efficiency, %	80
regenerator recycle fan electrical-mechanical efficiency, %	94
CO ₂ compression	
compressor isentropic efficiency, %	85
compressor electrical-mechanical efficiency, %	95
number of compressor stages	4
intercoolers outlet temperature, °C	35
after-cooler outlet temperature, °C	25
pump isentropic efficiency, %	80
pump electrical-mechanical efficiency, %	95
pressure drop in the intercoolers of compression and vacuum section	1% of the inlet pressure
minimum Pinch in the intercooler steam production	5 °C
low-pressure stream produced in modified scheme	saturated steam
Aspen property method	Peng–Robinson

^aThe mainstream data for the modified scheme is presented Table 3 (modified and optimized), while the mainstream data for the standard scheme is presented in Table S1, Supporting Information.

Two different process schemes for SARC integration with cement plant were evaluated in this study (Table 3). The standard scheme was introduced first by Cloete et al.²² for SARC integration to a cement plant (Figure S2, Supporting information). This scheme was modified (Figure 4) in this study to produce the low-pressure stream from the process itself and use that in the SARC regeneration reactor. The addition of steam promotes the CO₂ desorption during regeneration by reducing the CO₂ partial pressure²⁶ and can improve the techno-economic performance.

The modified scheme shown in Figure 4 introduces low-pressure saturated steam production from three different sections of the process. First, low-pressure saturated steam is produced from the surplus heat from the high-temperature circuit of the heat pump, which was rejected from the low-

temperature circuit of the heat pump in the standard scheme (Figure S2, Supporting Information). This slightly increases the heat pump consumption, while providing a considerable amount of steam. The second location for steam production is from the intercoolers of the CO₂ compression train and the vacuum pump. A subsequent cooler is still required after each intercooling boiler to minimize the stream temperature and the compressor duty. Third, additional steam is produced from cooling the flue gas stream. The produced steam was then fed to the desorber where it served to reduce the partial pressure of CO₂ (which allowed the desorption pressure to be increased from 0.1 to 0.2 bar) and to suppress H₂O desorption (which reduced the required heat duty to drive the endothermic desorption). The saturated steam was produced 0.2 bar higher than the desorption pressure to overcome the pressure drop in the reactor.

These two process models were evaluated for the cases presented in Table 4. The first five cases were studied with the standard process scheme (Figure S2, Supporting Information) while the last two cases were evaluated using the modified process scheme (Figure 4). From left to right, the cases in Table 4 can be described as follows: First, the benchmark case from the earlier techno-economic assessment of SARC²³ is simulated with the current process model for consistency. Next, the pressure drop is correctly accounted for in the model and the higher experimentally observed heat transfer coefficient is reflected. The third case increases the number of CSTRs in series to investigate the potential benefits of more inhibition of axial mixing, given the experimentally demonstrated simplicity of achieving this with perforated plates. Fourth, a more optimistic heat transfer coefficient (the upper bound of experimentally observed values) is investigated. The fifth case investigates the effect of shortening the reactor to lower the pressure drop and the reactor cost based on experimental observations²⁴ that the CO₂ adsorption is fast enough to reach equilibrium at only about half the default gas residence time used in the simulations. Sixth, the effect of injecting additional steam raised in the modified process scheme to the adsorption step is investigated. The final case combines all of the potential positive effects together to investigate the ultimate potential of the SARC process.

2.5. Process Economics. The methodology used in the economic assessment is unchanged from our previous work,²³ where the SARC concept was benchmarked under consistent assumptions against several competing technologies previously

Table 3. Properties of the Main Streams of the Modified Configuration with Steam Injection Shown in Figure 4 (Ideal Case)

stream	T, °C	P, bar	m, kg/s	mole fraction				
				CO ₂	H ₂ O	N ₂	O ₂	NH ₃
1	130	1.014	88.4	0.22	0.11	0.6	0.07	0
2	145.2	1.13	88.4	0.22	0.11	0.6	0.07	0
3	57.8	1.014	56.7	0.03	0.07	0.81	0.09	0
4	62.6	0.6	2.45	0.10	0.11	0.71	0.08	0
5	68.6	0.2	38	0.48	0.49	0.02	0.01	0
7	24	81.4	26.4	0.96	0.01	0.04	0.01	0
8	97.8	35.5	73.9	0	0	0	0	1
9	73.11	35.5	73.9	0	0	0	0	1
10	54.85	22.9	78.9	0	0	0	0	1
11	54.85	22.9	71	0	0	0	0	1
12'	97.8	35.5	5	0	0	0	0	1
13	54.85	23.9	78.92	0	0	0	0	1

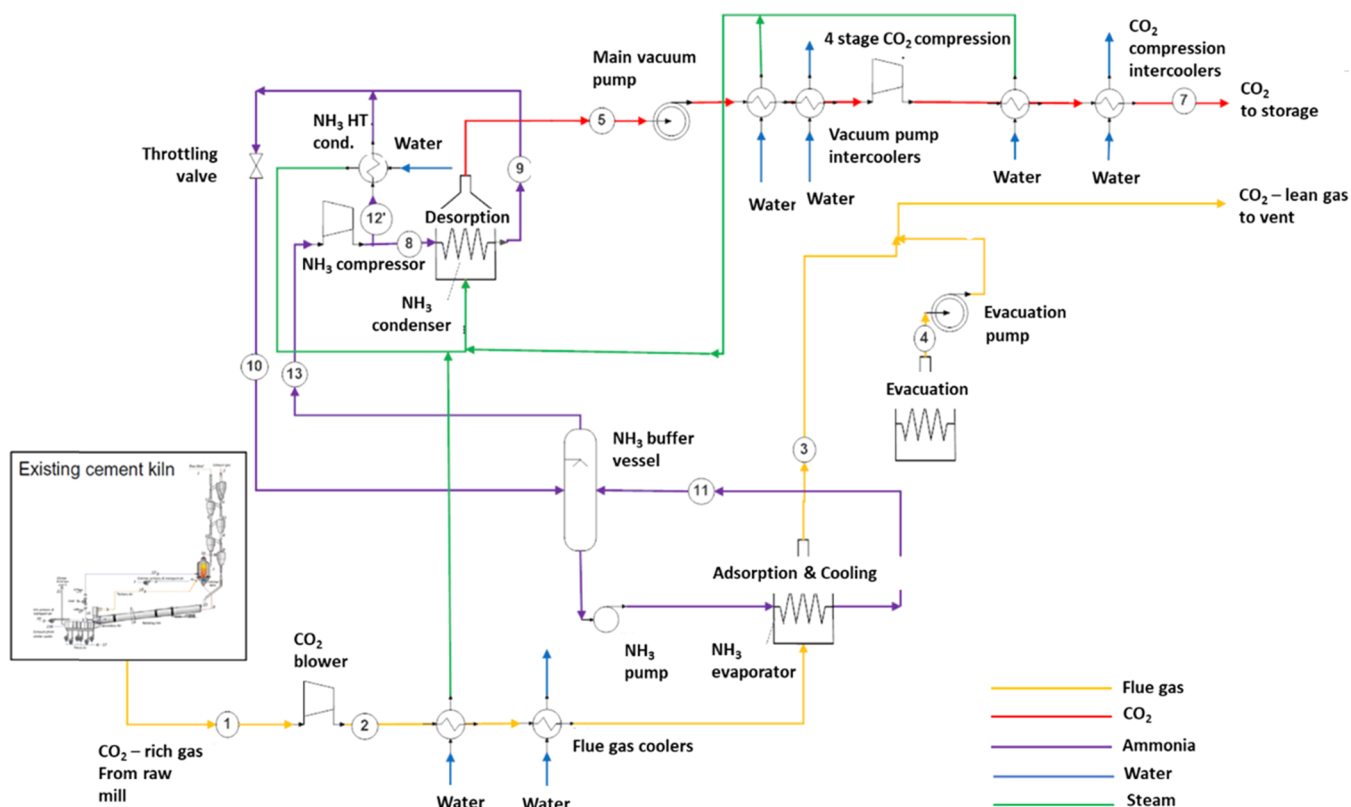


Figure 4. Modified process scheme with steam injection in SARC desorption step.

Table 4. Summary of Seven Cases Considered in This Study

case	original setup	PD & 400 W/(m ² K)	8 CSTRs	500 W/(m ² K)	half PD	steam	ideal
desorption pressure (bar)	0.1	0.1	0.1	0.1	0.1	0.2	0.2
heat transfer coefficient (W/(m ² K))	300	400	400	500	400	400	500
pressure drop (bar)	0.2	0.2	0.2	0.2	0.1	0.2	0.1
hydrostatic pressure included in model	no	yes	yes	yes	yes	yes	yes
number of CSTRs	4	4	8	4	4	4	8
steam addition in desorption	no	no	no	no	no	yes	yes

assessed in the CEMCAP project.²⁸ This study applies this established methodology to compare the CO₂ avoidance cost (CAC) resulting from the different cases detailed in Table 4. It is noted that the cost of large-scale vacuum pumps is an important uncertainty in this analysis, and we have used the most conservative option evaluated earlier²³ with no economies of scale beyond a flow rate of 500 (kg h)/kPa (the cases evaluated in this study would require 11–22 vacuum pumps at this maximum flow rate). Other important economic assumptions are detailed in Table 5.

3. RESULTS AND DISCUSSION

The results are presented in two sections. The first section reports the validation of the reactor model with the breakthrough experiments and the full SARC cycle, while the second section disseminates the results from the process and economic model for the seven cases in Table 4.

3.1. Validation Cases. **3.1.1. Breakthrough Experiments.** The first validation simulation evaluated the accuracy of the CSTR-in-series assumption. In the experiments, perforated plates are inserted to separate the reactor into four parts. However, the perforations are considerably larger than the particles, allowing for some particle exchange between the four

reactor stages. Because of this additional axial mixing between stages, it can be expected that the reactor will not show the ideal behavior expected from four CSTRs in series.

Figure 5 illustrates that this is indeed the case. The simulation with four CSTRs overpredicts the time before significant CO₂ breakthrough, which is an overly optimistic result. However, the simulation with three CSTRs achieves a close match to the experimental results. Given the practical simplicity of the solution for creating stages within the reactor, this is a very positive result. It should be simple and cheap to insert additional perforated plates in the reactor to further reduce the degree of axial mixing, implying that it may be possible to approach the ideal breakthrough curve of a fixed bed while maintaining the high heat transfer coefficients of a fluidized bed.

The overprediction of the reduction in axial mixing when four CSTRs are used in the simulation is confirmed in Figure 6. Clearly, the temperature wave takes a longer time to travel through the reactor in the simulation than the experiment. Due to the absence of separate pressure probes in each stage, it is not possible to directly quantify the sorbent distribution in the reactor, but the four successive peaks clearly indicate the presence of sorbent in each stage. However, the difference

Table 5. Summary of Key Economic Assumptions^a

plant economic lifetime	25 years
construction period	3 years
capacity factor	91.3%
discount rate	8%
process contingencies	
reactors (including heat exchangers)	40% of installed costs
all other equipment	20% of installed costs
plant contingency (all equipment)	12% of installed costs
project contingency	15% of total direct costs
indirect costs	14% of total direct costs
owner's costs	7% of total direct costs
maintenance, insurance, and taxes	4.5% of total plant costs per year
labor costs	3.2% of total plant costs per year
sorbent cost	€15/kg
sorbent lifetime	2 years
electricity costs	€58.1/MWh
indirect CO ₂ from electricity consumption	262 kg/MWh

^aInstalled costs = base cost of fully installed equipment. Total direct costs = installed costs plus process and plant contingencies. Total plant costs = total direct costs plus project contingency and indirect and owner's costs.

between experimental and simulation results becomes most apparent in the fourth stage, indicating that the amount of sorbent in the final two stages may be lower (as opposed to the constant sorbent loading in each stage assumed in the simulation). A greater concentration of sorbent in the bottom three stages offers another explanation for why the simulation using only three CSTRs produced a more accurate breakthrough curve than the simulation with four CSTRs. Figure 6 also shows that the model achieves a reasonable prediction of the local temperature rise due to the exothermic reaction as the reaction front moves through the different reactor stages, heating the bed faster than the cooling oil can remove heat.

Based on these results, the comparison to the full SARC cycle presented next will be carried out using only three CSTRs to correctly predict the degree of plug flow achieved in the experimental setup.

3.1.2. Full SARC Cycle. The most important aspect that the model must capture is the degree of CO₂ capture achieved in the adsorption step. As shown in Figure 7, the CO₂ slippage during adsorption is accurately predicted. This result is achieved through a combination of three effects: (1) the rapid adsorption kinetics that justifies the assumption of equilibrium conversion in the model, (2) the correct degree of plug flow achieved by simulating three CSTRs to represent the experiment four-stage reactor, and (3) accurate heat transfer predictions to achieve the right temperatures in the different reactor stages and steps.

When considering the temperature profiles in Figure 8, a reasonable match is achieved aside from the reactor heating in the long desorption step (240–1140 s). Heat transfer in the desorption step was complicated by defluidization of the lowest reactor stage in the experiments due to an insufficient rate of CO₂ release. This is a self-strengthening effect: less fluidization causes poorer heat transfer, slowing down the temperature increase needed to drive the CO₂ release required to fluidize the reactor. Thus, a clear threshold will exist beyond which this effect is activated and the bed defluidizes.

A constant average heat transfer coefficient was derived from experimental data for each of the lower three reactor stages: 192, 338, and 343 W/(m² K) from the bottom to the top. This result clearly shows the poorer fluidization in the lower stage, leading to a lower heat transfer coefficient. The second and third stages show higher heat transfer coefficients, indicating that they are successfully fluidized, aided by the CO₂ release in lower stages. Heat transfer coefficients in the bottom three stages for the adsorption and cooling steps were measured as 508 and 393 W/(m² K), respectively.

For most of the desorption step, the heat transfer coefficient in the bottom stage was only around 50 W/(m² K), indicating very poor fluidization. However, at the start of the desorption step, the heat transfer coefficient was similar to the second and third stages due to the faster initial release of CO₂ when the sorbent is still highly carbonated; this results in the average heat transfer coefficient of 192 W/(m² K) that was implemented in the simulation.

The trends in Figure 8 during the desorption step (240–1140 s) illustrate the effects of this simplification. Initially, the

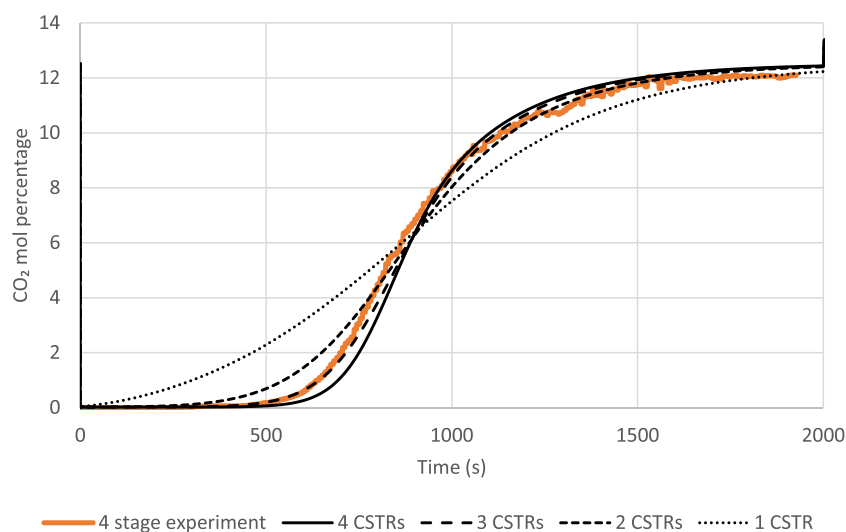


Figure 5. Effect of the number of CSTRs in series on the simulated breakthrough curve, compared to experimental data with and without stage separators in the reactor.

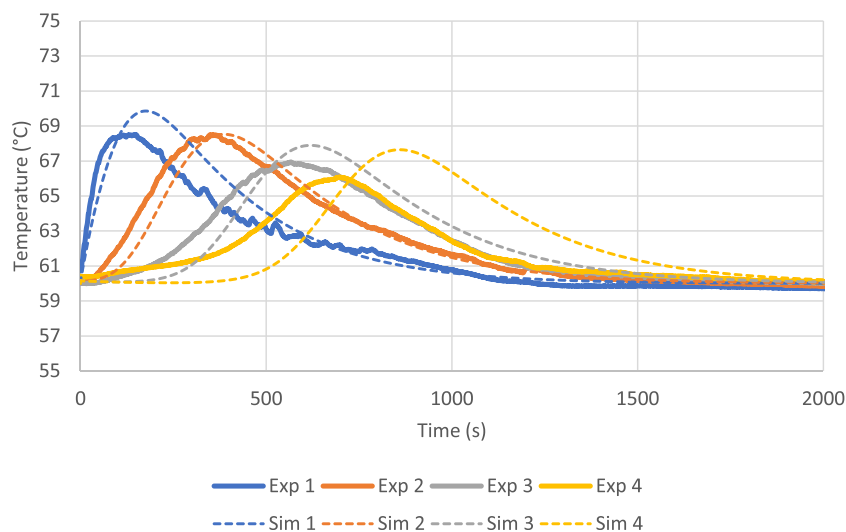


Figure 6. Comparison between simulated and experimental measurements of temperature in the four reactor stages. The numbers in the legend indicate the four reactor stages.

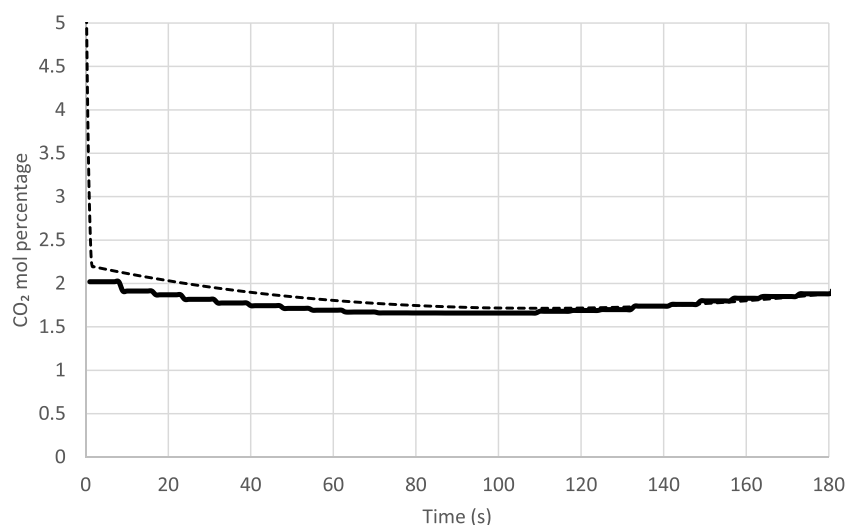


Figure 7. Simulated CO_2 mol fraction at the outlet of the adsorption step compared to experimental measurements from a full SARC cycle.

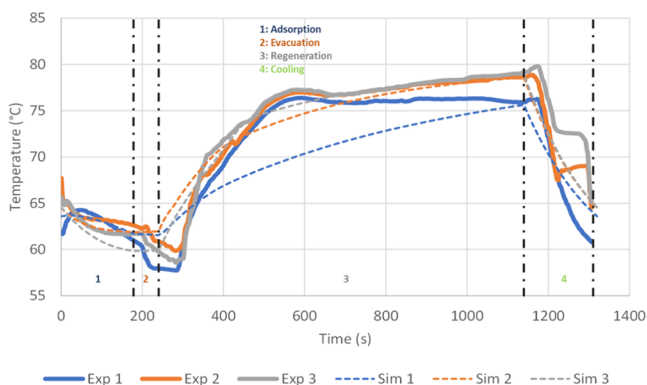


Figure 8. Comparison of simulated (Sim) temperature profiles to experimental (Exp) measurements over a full SARC cycle. The numbers in the legend indicate the three reactor stages.

first stage (blue lines) temperature rise in the experiments is much faster than the simulation prediction. This is the result of the higher heat transfer coefficient observed at the start of the desorption step when this stage was successfully fluidized. As

the desorption step progresses, the experimental heat transfer coefficient sharply reduces as the first stage defluidizes and the simulation catches up due to the average heat transfer coefficient implemented. Ultimately, the correct final temperature is reached, causing the right degree of desorption in the simulated SARC cycle.

Figure 8 also shows a delay in the experimental temperature rise at the start of the desorption step (240 s) and the temperature fall at the start of the cooling step (1140 s). This is the result of the delay in switching the heating oil pumps and displacing the cold oil with the hot oil when switching to desorption (and vice versa when switching to cooling).

Another observation from the experimentally measured heat transfer coefficients is that the top stage consistently showed worse heat transfer performance. During adsorption, desorption, and cooling, the heat transfer coefficient in the top stage was, respectively, 46, 34, and 73% lower than in the third stage. This supports the discussion around Figure 6 that the top stage contains fewer particles, even during adsorption when the gas flow rate is relatively high. During cooling, the fluidization velocity is considerably smaller, causing the bed to become

more compact and particles to rain down from the top stage to the third stage, causing the large observed reduction in the top stage heat transfer coefficient. These observations provide further explanation for why the simulation with only three CSTRs in series provided the best match to experimental results.

In summary, the key modeling aspects that were successfully validated over the full SARC cycle in this campaign include:

- Rapid experimentally observed adsorption and desorption rates led to good CO₂ capture performance predictions from the model based on the assumption of equilibrium CO₂ concentrations in each CSTR.
- The simple perforated plates in the experimental reactor could closely replicate the behavior of perfectly separated CSTRs in the modeling. Results suggest that the primary reason why three CSTRs in the modeling best approximated the four-stage experimental reactor behavior was a lower particle loading in the top stage.
- High heat transfer coefficients of up to 500 W/(m² K) could be achieved experimentally. Implementation of the measured heat transfer coefficients led to good model predictions of the temperature at the end of each step in the cycle, thus leading to accurate predictions of overall adsorption and desorption in each step. Desorption was the only reactor step with poor heat transfer performance due to insufficient CO₂ release in the bottom stage that resulted in defluidization. Such defluidization can be prevented by feeding a small amount of recirculated CO₂ or vacuum pressure steam raised from heat integration to the regeneration step.

With these key model assumptions successfully verified via experiments, the model can now be used to refine a prior economic assessment of the SARC concept. The cases in Table 4 were defined to explore the implications of the learnings from this experimental study on the simulated techno-economic performance of the large-scale SARC process. These results are presented and discussed in the following section.

3.2. Economic Implications of Experimental Observations. The simulations were completed using six new cases and compared to the original setup as summarized in Table 4. The CO₂ avoidance cost (CAC) for the seven cases is presented in Figure 9. The CAC with the standard process scheme based on the original reactor model is €51/ton CO₂, which is €1/ton lower than the previous study²³ due to a change in the CO₂ adsorption isotherm. Correctly modeling the effect of pressure drop (PD and 400 W/(m² K)) increased the CAC by 4.8% compared to the original setup case. This increase in CAC occurred despite increasing the heat transfer coefficient from 300 to 400 W/(m² K), indicating the significant negative effect that higher pressures in the lower reactor stages have on desorption performance. Figure 10a shows that this increase is due to a substantial increase in heat pump power consumption required to drive the larger temperature swing needed to compensate for the higher desorption pressures in the lower reactor stages. Figure 10b shows that the increase in capital cost associated with the larger ammonia compressor is negligible.

Next, the positive effects of increasing the number of CSTR in the reactor model and further increasing the heat transfer coefficient are investigated. Both cases reduced the CAC but it remained higher by 2 and 2.8% compared to the original setup

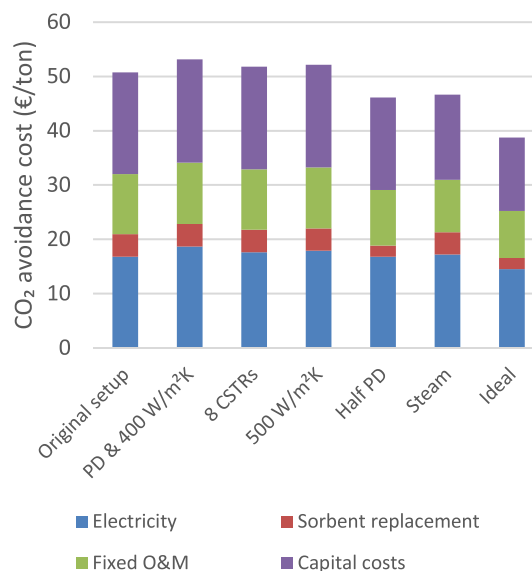


Figure 9. CO₂ avoidance cost for seven cases detailed in Table 4.

case. Both these cases reduce the required temperature swing and thus the heat pump consumption (Figure 10a), but it is clear that the gains achievable from further reducing axial mixing and increasing the heat transfer coefficient are minor.

Halving the reactor height had a considerably larger effect, reducing the CAC by 9.1% compared to the original setup and 13.3% compared to the case with full pressure drop. This modification had multiple advantageous effects on the process economics. First, the consumption of the flue gas blower was reduced due to the lower reactor pressure drop. Second, heat pump consumption also reduced due to the reduced negative effect of the hydrostatic pressure increase in the lower reactor regions. Third, the cost of the reactor vessels reduced due to their lower height. Fourth, the sorbent cost was halved because only half the sorbent is used in the reactor. Figure 10 shows that the reduction in capital cost is significantly larger than the reduction in electricity consumption. Sorbent cost reductions also play an important role by reducing both the sorbent replacement costs in Figure 9 and the cost of the original batch of sorbent included in the capital costs (Figure 10b).

An almost similar reduction in CAC (8%) was observed with the modified process scheme (Figure 4), where the steam is fed to the SARC desorption step. The reduction in vacuum pump costs, enabled by an increase in desorption pressure from 0.1 to 0.2 bar, is the major benefit of this case. As shown in Figure 10a, the additional partial pressure swing enabled by the steam addition allowed the vacuum pump pressure to be reduced without excessive increases in heat pump consumption, keeping the total power consumption similar to prior cases. Without this added partial pressure swing, increasing the desorption pressure negatively affects the economic performance of the process.²³

When all positive effects are combined in the ideal case, a large reduction in CAC of 23.7% is observed. This brings the CAC to €38.7/ton, which is well below the most economical benchmark (oxyfuel combustion) at €42.4/ton.²⁸ The main contributors to this large cost reduction are the cheaper vacuum pump caused by the steam injection, the lower reactor and sorbent costs from the smaller reactor size, and the reduced power consumption from the blower.

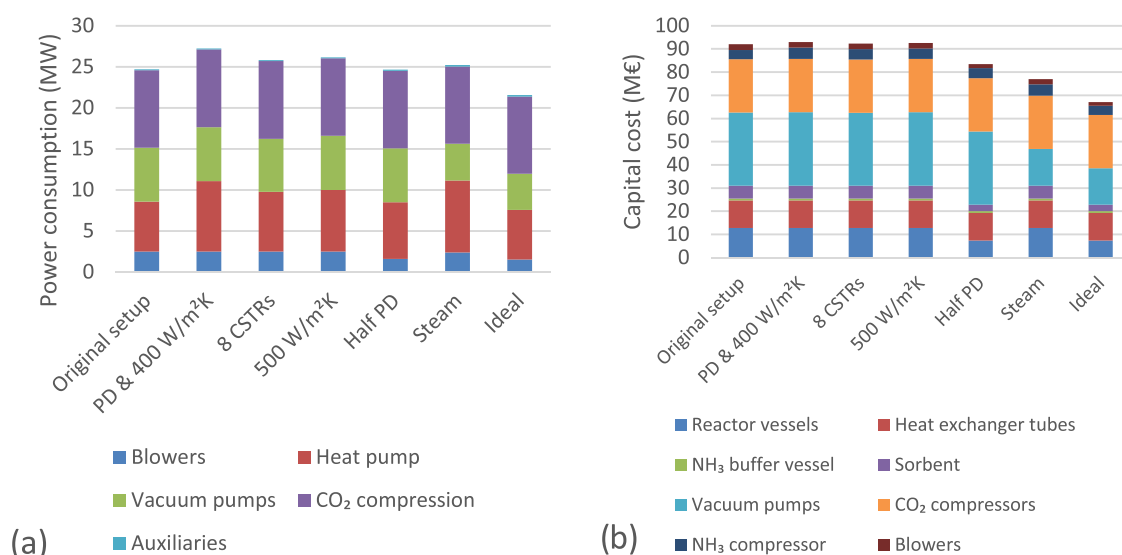


Figure 10. Breakdown of (a) power consumption and (b) capital cost of the seven cases detailed in Table 4.

Finally, attention should be drawn to an important economic uncertainty parameter identified from the experimental campaign. In the economic assessment, a sorbent lifetime of 2 years is assumed, but the experimental results indicated a rate of fines elutriation of 0.09%/h, which translates into a lifetime of only 7.2 weeks at a capacity factor of 91.3%. As shown in Figure 11a, such a short sorbent lifetime will compromise the economic competitiveness of the SARC process.

Once commercialized, the ease of retrofitting and independence of process heat offered by SARC may make it competitive for some applications even at a CAC of €55/ton.²³ When using the default sorbent cost of €15/kg, the sorbent lifetime should be improved by a factor of 1.6–4.8 over the observations from this study depending on whether the combination of steam integration and short reactor height in the ideal case proves feasible. From a number of studies reviewed by Thon and Werther,²⁹ mature fluidized bed catalysts typically have attrition rates in the order of $1 \times 10^8 \text{ s}^{-1}$ under bubbling fluidization, translating to a durability of about 3.5 years (25× longer than observed in this study). Substantial gains in mechanical stability can therefore be expected once this is identified as the primary economic requirement for SARC and other sorbent-based CO₂ capture processes.

It is therefore clear that the development of a more mechanically robust sorbent is of high priority for realizing the great techno-economic potential of the SARC concept shown in Figure 9. Furthermore, the chemical stability of the sorbent using real flue gases with high O₂ concentrations and traces of other pollutants must be demonstrated under real SARC operating conditions. The thermal stability issues of PEI sorbents are inherently avoided by the SARC process due to its mild desorption temperatures enabled by the vacuum swing.

Figure 11 also illustrates several other sensitivities to model parameters varied over a range of $\pm 50\%$. The effect of sorbent cost (Figure 11b) increases as the sorbent lifetime reduces from 2 years to 6 months. This sensitivity reduces for the ideal case because the shorter bed halves the sorbent inventory in the reactors. Figure 11c shows that the CAC is only mildly sensitive to the costs of the two most uncertain units in the plant: the SARC reactor cluster and the vacuum pump. A

higher sensitivity is observed when the discount rate is varied between 4 and 12%. The sensitivity to electricity costs in Figure 11d is similar across the two cases and the three CO₂ emissions intensities investigated. The CO₂ emissions intensity of the electricity has a significant effect on CAC because indirect emissions from electricity consumption reduce the total avoided CO₂, thereby increasing the cost per unit avoided CO₂.

4. CONCLUSION

It is common practice to complete techno-economic assessments of new process concepts using idealized modeling assumptions such as perfect reactor mixing and chemical equilibrium. This practice was also followed in previous publications to assess the potential of the SARC post-combustion CO₂ capture technology. In this study, the reactor model used in previous works was validated against experimental data collected from a lab-scale multistage fluidized bed reactor used to demonstrate the SARC concept.

In general, the comparison showed that the previously employed reactor model assumptions were reasonable. The most important correction to the reactor model that proved necessary was to account for the effect of the hydrostatic pressure gradient in the lower regions of the reactor which significantly suppressed desorption, negatively affecting reactor performance. On the positive side, the previously published experimental results showed that a substantially higher heat transfer coefficient could be achieved in practice than originally assumed in the reactor simulations, that limiting axial sorbent mixing using simple porous separators was highly effective, and that the adsorption reaction was fast enough to justify the modeling assumption of chemical equilibrium.

These learnings from the experimental campaign were used to revise the reactor model and quantify the impacts of these revisions on the projected economic performance of the SARC concept. It was shown that the negative effect of pressure drop outweighed the positive effect of increased heat transfer to increase the CO₂ avoidance cost (CAC) by 4.8 and 2.8% in the lower and upper ranges of the observed experimental heat transfer coefficient, respectively. Capitalizing on the simplicity of further reducing axial solids mixing to delay the CO₂

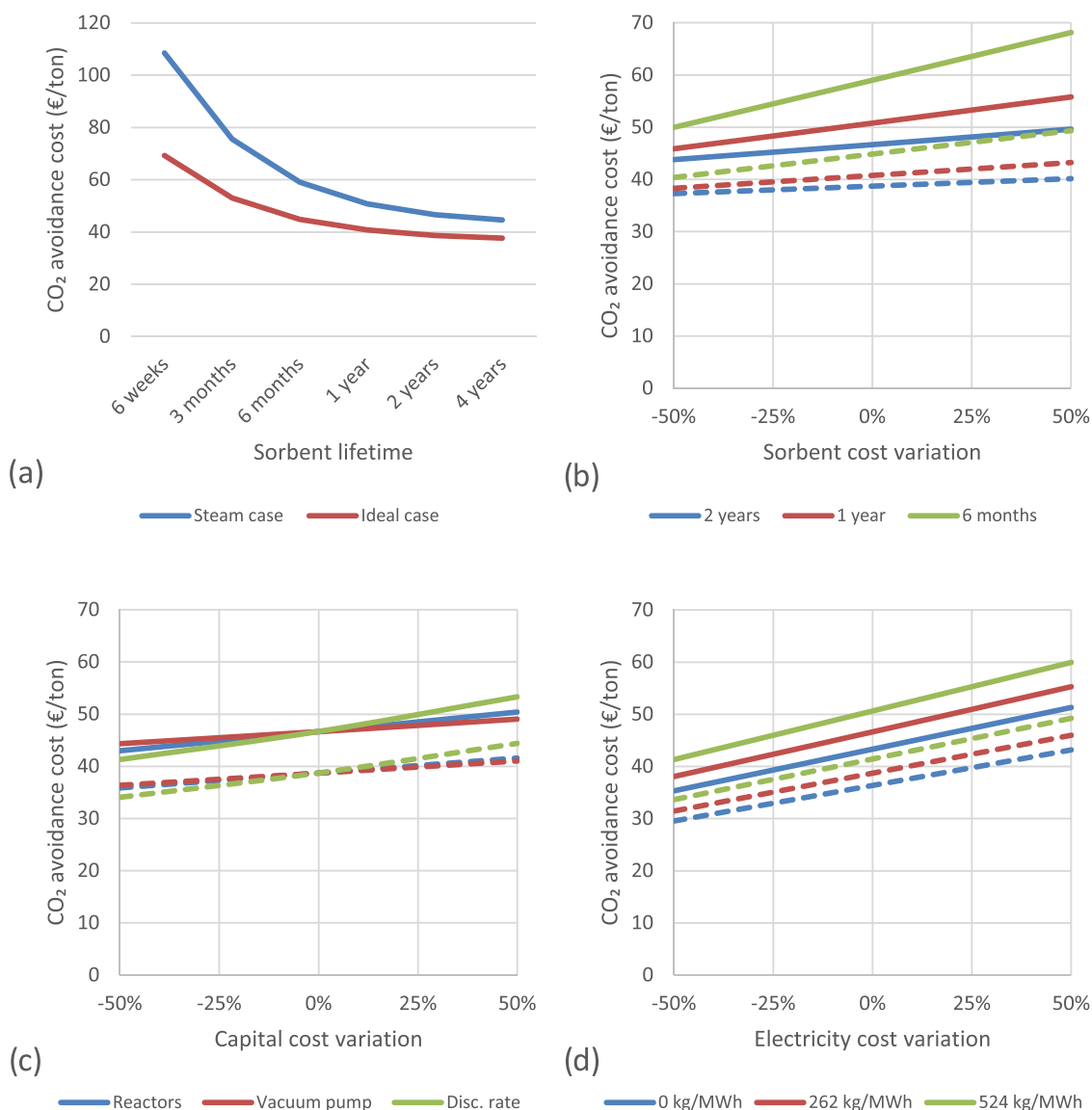


Figure 11. Sensitivity of the CAC to various model assumptions for the “Steam” (solid lines) and “Ideal” (dashed lines) cases in Table 4. Base assumptions are 2 years sorbent lifetime, €15/kg sorbent cost, 8% discount rate, and €58.1/MWh electricity cost.

breakthrough only brought small gains by reducing the CAC by 2.8%. The potential of constructing shorter reactors to capitalize on the fast adsorption kinetics observed in the experiments had a much larger effect, reducing the CAC by 13.3%, illustrating the importance of minimizing reactor size and pressure drop. Optimizing the trade-off between reactor size and gas-solid contact time is therefore an important priority for future work.

In addition, a new heat integration scheme was investigated where very low-pressure steam was raised from several low-grade heat sources in the SARC plant, still avoiding any need for heat integration with the host process. This process integration reduced the CAC almost as much as halving the reactor size, demonstrating that this relatively simple heat integration scheme should be the default configuration in future SARC plants. When this new heat integration layout was combined with all of the aforementioned potential gains in economic performance, the optimal CAC emerged to be 23.7% below the case with the original SARC reactor model. This CAC of €38.7/ton is significantly below the most economical

solution for new cement plants, oxyfuel combustion, illustrating the potential of SARC to be the preferred solution not only for retrofits but for greenfield plants as well.

Finally, attention was drawn to a key uncertainty in the economic performance of the SARC concept: sorbent durability. The observed fines generation rate from the experiments is well above the assumption in the modeling and would strongly reduce economic performance. The development of more mechanically robust sorbents should therefore be a high priority to realize the potential of this promising post-combustion CO₂ capture concept. In addition, long-term demonstration of chemical stability in real flue gases is another high sorbent-related priority.

■ ASSOCIATED CONTENT

SI Supporting Information


The Supporting Information is available free of charge at <https://pubs.acs.org/doi/10.1021/acs.iecr.1c00357>.

Descriptions of the SARC experimental setup and operating procedure, images of the setup, the standard

scheme for SARC integration to cement plant, and details of major streams in standard scheme (PDF)

AUTHOR INFORMATION

Corresponding Author

Abdelghafour Zaabout – Process Technology Group, SINTEF Industry, Trondheim 7031 Trøndelag, Norway;
 orcid.org/0000-0002-7468-8050; Phone: +47 930 08 204; Email: abdelghafour.zaabout@sintef.no

Authors

Chaitanya Dhoke – Norwegian University of Science and Technology, Trondheim 7034 Trøndelag, Norway;

 orcid.org/0000-0001-5580-1962

Schalk Cloete – Process Technology Group, SINTEF Industry, Trondheim 7031 Trøndelag, Norway

Shahriar Amini – Norwegian University of Science and Technology, Trondheim 7034 Trøndelag, Norway;
 Department of Mechanical Engineering, University of Alabama, Tuscaloosa, Alabama 35401, United States

Complete contact information is available at:
<https://pubs.acs.org/10.1021/acs.iecr.1c00357>

Notes

The authors declare no competing financial interest.

ACKNOWLEDGMENTS

This study was performed as part of the project entitled “Demonstration of the Swing Adsorption Reactor Cluster (SARC) for simple and cost-effective post-combustion CO₂ capture”, funded by the Research Council of Norway under the CLIMIT program (Grant no. 268507/E20). The assistance of technical staff at the VATL lab (Reidar Tellebon, Inge Håvard Rekstad, Sondre Hoelstad Nubdal, Aleksander Mosand, Bendik Sægrov, and Morten Grønli) in constructing and maintaining the lab-scale reactor is greatly appreciated. The time and efforts deployed by the reviewers for reviewing this manuscript is also greatly appreciated.

LIST OF ACRONYMS

SARC	swing adsorption reactor cluster
VTSA	vacuum combined temperature swing adsorption
MFC	mass flow controller
PEI	polyethyleneimine
LPM	liters per minute
EXP 1– EXP 4	temperature inside stage 1 to stage 4 of the reactor measured experimentally
SIM 1- SIM 4	temperature inside stage 1 to stage 4 of the reactor estimated from reactor model
CSTR	continuous stirred tank reactor

REFERENCES

- (1) Samanta, A.; Zhao, A.; Shimizu, G. K. H.; Sarkar, P.; Gupta, R. Post-Combustion CO₂ Capture Using Solid Sorbents: A Review. *Ind. Eng. Chem. Res.* **2012**, *51*, 1438–1463.
- (2) Webley, P. A. Adsorption technology for CO₂ separation and capture: a perspective. *Adsorption* **2014**, *20*, 225–231.
- (3) Abanades, J. C.; Arias, B.; Lyngfelt, A.; Mattisson, T.; Wiley, D. E.; Li, H.; Ho, M. T.; Mangano, E.; Brandani, S. Emerging CO₂ capture systems. *Int. J. Greenhouse Gas Control* **2015**, *40*, 126–166.
- (4) Ben-Mansour, R.; Habib, M. A.; Bamidele, O. E.; Basha, M.; Qasem, N. A. A.; Peedikakkal, A.; Laoui, T.; Ali, M. Carbon capture

by physical adsorption: Materials, experimental investigations and numerical modeling and simulations – A review. *Appl. Energy* **2016**, *161*, 225–255.

(5) Omodolor, I. S.; Otor, H. O.; Andonegui, J. A.; Allen, B. J.; Alba-Rubio, A. C. Dual-Function Materials for CO₂ Capture and Conversion: A Review. *Ind. Eng. Chem. Res.* **2020**, *59*, 17612–17631.

(6) Danaci, D.; Bui, M.; Mac Dowell, N.; Petit, C. Exploring the limits of adsorption-based CO₂ capture using MOFs with PVSA - from molecular design to process economics. *Mol. Syst. Des. Eng.* **2020**, *5*, 212–231.

(7) Dhoke, C.; Zaabout, A.; Cloete, S.; Amini, S. Review on Reactor Configurations for Adsorption-Based CO₂ Capture. *Ind. Eng. Chem. Res.* **2021**, *60*, 3779–3798.

(8) Webley, P. A.; Zhang, J. Microwave assisted vacuum regeneration for CO₂ capture from wet flue gas. *Adsorption* **2014**, *20*, 201–210.

(9) Luberti, M.; Oreggioni, G. D.; Ahn, H. Design of a rapid vacuum pressure swing adsorption (RVPISA) process for post-combustion CO₂ capture from a biomass-fuelled CHP plant. *J. Environ. Chem. Eng.* **2017**, *5*, 3973–3982.

(10) Rezaei, F.; Grahn, M. Thermal Management of Structured Adsorbents in CO₂ Capture Processes. *Ind. Eng. Chem. Res.* **2012**, *51*, 4025–4034.

(11) Rezaei, F.; Mosca, A.; Webley, P.; Hedlund, J.; Xiao, P. Comparison of Traditional and Structured Adsorbents for CO₂ Separation by Vacuum-Swing Adsorption. *Ind. Eng. Chem. Res.* **2010**, *49*, 4832–4841.

(12) Gupta, T.; Ghosh, R. Rotating bed adsorber system for carbon dioxide capture from flue gas. *Int. J. Greenhouse Gas Control* **2015**, *32*, 172–188.

(13) Grande, C. A.; Kvamsdal, H.; Mondino, G.; Blom, R. Development of Moving Bed Temperature Swing Adsorption (MBTSA) Process for Post-combustion CO₂ Capture: Initial Benchmarking in a NGCC Context. *Energy Procedia* **2017**, *114*, 2203–2210.

(14) Kim, K.; Son, Y.; Lee, W. B.; Lee, K. S. Moving bed adsorption process with internal heat integration for carbon dioxide capture. *Int. J. Greenhouse Gas Control* **2013**, *17*, 13–24.

(15) Okumura, T.; Ogino, T.; Nishibe, S.; Nonaka, Y.; Shoji, T.; Higashi, T. CO₂ Capture Test for A Moving-bed System Utilizi g Low-temperature Steam. *Energy Procedia* **2014**, *63*, 2249–2254.

(16) Kim, J.-Y.; Woo, J.-M.; Jo, S.-H.; Lee, S.-Y.; Moon, J.-H.; Kim, H.; Yi, C.-K.; Lee, H.; Snape, C. E.; Stevens, L.; Sun, C.; Liu, H.; Liu, J.; Park, Y. C. Continuous testing of silica-PEI adsorbents in a lab-scale twin bubbling fluidized-bed system. *Int. J. Greenhouse Gas Control* **2019**, *82*, 184–191.

(17) Yi, C.-K.; Jo, S.-H.; Seo, Y.; Lee, J.-B.; Ryu, C.-K. Continuous operation of the potassium-based dry sorbent CO₂ capture process with two fluidized-bed reactors. *Int. J. Greenhouse Gas Control* **2007**, *1*, 31–36.

(18) Roy, S.; Mohanty, C. R.; Meikap, B. C. Multistage Fluidized Bed Reactor Performance Characterization for Adsorption of Carbon Dioxide. *Ind. Eng. Chem. Res.* **2009**, *48*, 10718–10727.

(19) Schöny, G.; Dietrich, F.; Fuchs, J.; Pröll, T.; Hofbauer, H. A multi-stage fluidized bed system for continuous CO₂ capture by means of temperature swing adsorption – First results from bench scale experiments. *Powder Technol.* **2017**, *316*, 519–527.

(20) Zaabout, A.; Romano, M. C.; Cloete, S.; Giuffrida, A.; Morud, J.; Chiesa, P.; Amini, S. Thermodynamic assessment of the swing adsorption reactor cluster (SARC) concept for post-combustion CO₂ capture. *Int. J. Greenhouse Gas Control* **2017**, *60*, 74–92.

(21) Zhao, Q.; Wu, F.; Men, Y.; Fang, X.; Zhao, J.; Xiao, P.; Webley, P. A.; Grande, C. A. CO₂ capture using a novel hybrid monolith (H-ZSM5/activated carbon) as adsorbent by combined vacuum and electric swing adsorption (VESA). *Chem. Eng. J.* **2019**, *358*, 707–717.

(22) Cloete, S.; Giuffrida, A.; Romano, M. C.; Zaabout, A. The swing adsorption reactor cluster for post-combustion CO₂ capture from cement plants. *J. Cleaner Prod.* **2019**, *223*, 692–703.

(23) Cloete, S.; Giuffrida, A.; Romano, M. C.; Zaabout, A. Economic assessment of the swing adsorption reactor cluster for CO₂ capture from cement production. *J. Cleaner Prod.* **2020**, *275*, No. 123024.

(24) Dhoke, C.; Zaabout, A.; Cloete, S.; Seo, H.; Park, Y.-k.; Demoulin, L.; Amini, S. Demonstration of the Novel Swing Adsorption Reactor Cluster Concept in a Multistage Fluidized Bed with Heat-Transfer Surfaces for Postcombustion CO₂ Capture. *Ind. Eng. Chem. Res.* **2020**, 22281.

(25) Dhoke, C.; Zaabout, A.; Cloete, S.; Seo, H.; Park, Y.-k.; Blom, R.; Amini, S. The swing adsorption reactor cluster (SARC) for post combustion CO₂ capture: Experimental proof-of-principle. *Chem. Eng. J.* **2019**, *377*, No. 120145.

(26) Dhoke, C.; Cloete, S.; Krishnamurthy, S.; Seo, H.; Luz, I.; Soukri, M.; Park, Y.-k.; Blom, R.; Amini, S.; Zaabout, A. Sorbents screening for post-combustion CO₂ capture via combined temperature and pressure swing adsorption. *Chem. Eng. J.* **2020**, *380*, No. 122201.

(27) Cloete, S.; Giuffrida, A.; Romano, M. C.; Zaabout, A. The effect of sorbent regeneration enthalpy on the performance of the novel Swing Adsorption Reactor Cluster (SARC) for post-combustion CO₂ capture. *Chem. Eng. J.* **2019**, *377*, No. 119810.

(28) Gardarsdottir, S. O.; Romano, M.; Roussanaly, S.; Voldsund, M.; Pérez-Calvo, J.-F.; Berstad, D.; Fu, C.; Anantharaman, R.; Sutter, D.; Gazzani, M.; De Lena, E. Comparison of Technologies for CO₂ Capture from Cement Production—Part 2: Cost Analysis. *Energies* **2019**, *12*, 542.

(29) Thon, A.; Werther, J. Attrition resistance of a VPO catalyst. *Appl. Catal., A* **2010**, *376*, 56–65.